Journal of Alloys and Compounds 509 (2011) 3052–3056

Contents lists available at ScienceDirect

Journal of Alloys and Compounds

journal homepage: www.elsevier.com/locate/jallcom

Influence of imidazolium-based ionic liquids on the performance of polyaniline–$CoFe_2O_4$ nanocomposites

Chunjiang Leng, Jianhong Wei*, Zhengyou Liu, Jing Shi

Key Laboratory of Artificial Micro- and Nano-structures of Ministry of Education and School of Physics and Technology, Wuhan University, Wuhan 430072, China

ARTICLE INFO

Article history:
Received 1 September 2010
Received in revised form
29 November 2010
Accepted 30 November 2010
Available online 7 December 2010

Keywords:
Polymer
Nanocomposite
Chemical synthesis
Conductivity
Magnetization

ABSTRACT

Using cobalt ferrite ($CoFe_2O_4$) nanoparticles of different content as nucleation sites, polyaniline–$CoFe_2O_4$ nanofiber composites were successfully synthesized at the interface of water and ionic liquid via in-situ polymerization. Structure and morphology were investigated by TGA, TEM, XRD, and FT-IR. The influence of ionic liquids on the structure, conductivity and magnetic property of polyaniline–$CoFe_2O_4$ nanocomposites were studied in detail. The results show that imidazolium-based ionic liquids $BMIPF_6$ acts as an anchor agent during the nanofiber composites formation process. Introduction of ionic liquids obviously improves the conductivity but weakens the magnetization of polyaniline–$CoFe_2O_4$ nanocomposites in the same [$CoFe_2O_4$]/[An] ratio.

1. Introduction

Recently, inorganic-organic nanocomposites with controllable electric and magnetic properties have attracted increasing attention because of their unique magnetic, electrical and optical properties and their potential application in electric catalysis, chemical sensors and photoelectric devices [1–4]. Multicomponent conducting polymer systems with nanoparticles of metal oxides not only can be tailored to obtain desired electrical or magnetic properties, but also can control the growth of inorganic oxides to yield uniform overall size distribution.

Among various conducting polymers, polyaniline (PANI) is one of the most promising conducting polymers because of its unique electrical, optical, and optoelectric properties, as well as its ease of preparation and excellent environmental stability [5–7]. Being a magnetic materials, cobalt ferrite ($CoFe_2O_4$) is one of the most important spinel ferrites with a Curie temperature around 793 K. The material shows a relatively large magnetic hysteresis which distinguishes it from other spinel ferrites. Recently, $CoFe_2O_4$ has been consider for various applications such as high density recording media and magnetic fluids because of its large magnetocrystalline anisotropy, high coercivity, moderate saturation magnetization, large magnetostrictive coefficient, chemical stability and mechanical hardness etc [8–12]. Electromagnetic functionality of nanostructure conducting polymers has attracted considerable attention because of their promising potential applications as electromagnetic interference shielding, microwave absorption materials, and anti-corrosion materials [13–16], etc. Up to now, a number of articles have been published on the magnetic and conducting polymeric nanocomposites of PANI as well as polypyrrole composites containing nanoparticles such as $BaFe_{12}O_{19}$, $MgFe_2O_4$, Fe_3O_4, and $CoFe_2O_4$ [17–21]. However, to our best knowledge, there is no report on the conducting polymer/ferrite composites prepared in ionic liquids until now.

Parallel to the development of the above nanocomposites, the topic of "green" chemistry and chemical processes has been emphasized. Room temperature ionic liquids, which are organic salts and liquids at room temperature, have attracted much attention as promising green solvents because of their unique properties such as excellent thermal stability, low volatility, wide electrochemical potential windows, and special solubility properties. In particular, imidazolium ionic liquids associated with specific anions are known to self-organize in a way that is adaptable to the fabrication of nanostructures of conducting polymers and inorganic materials [22–25].

In the present work, we describe a facile and eco-friendly method of synthesizing PANI–$CoFe_2O_4$ nanocomposites at the interface of water and ionic liquid. The influence of imidazolium-based ionic liquids on the morphology, structure, conductivity, and magnetic properties of PANI–$CoFe_2O_4$ nanocomposites were investigated in detail. In general, the preparation of organic-inorganic composites often results in pollution. This route is expected to have

* Corresponding author. Tel.: +86 27 68754613; fax: +86 27 68752569.
E-mail address: jhwei@whu.edu.cn (J. Wei).

0925-8388/$ – see front matter © 2010 Elsevier B.V. All rights reserved.
doi:10.1016/j.jallcom.2010.11.197

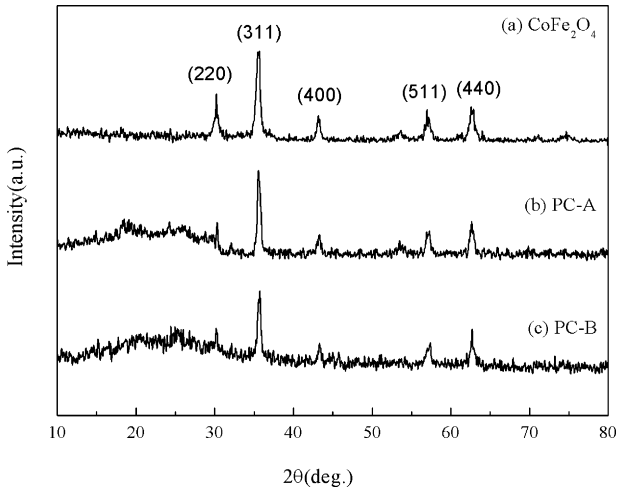

Fig. 1. XRD spectra of (a) $CoFe_2O_4$ particles, (b) PC-A, (c) PC-B.

a reduced pollution effect during materials preparation because both water and ionic liquid are environmentally benign solvents.

2. Experimental

2.1. Preparation

In the experiment, $CoFe_2O_4$ nanoparticles were prepared by the hydrothermal method using sodium bis (2-ethylhexyl) sulphosuccinate (AOT) as the surfactant. Firstly, 80 ml aqueous solutions contain 0.01 mol $CoCl_2{\cdot}6H_2O$, 0.02 mol $FeCl_3{\cdot}6H_2O$, and 0.5 g AOT were added drop by drop into 20 ml 1.625 M NaOH aqueous solutions under vigorous stirring at 95 °C. After continuous stirring for 0.5 h, the brown suspension obtained was transferred into 150 ml autoclaves, after which the autoclave was sealed and put into an oven heated at 200 °C for 10 h and cooled naturally to room temperature. Finally, the black suspension obtained was washed with distilled water and ethanol several times to remove the impurities and dried in the oven at 100 °C for 2 h.

In the case of the preparation of PANI–$CoFe_2O_4$ composites, 1 g as-prepared $CoFe_2O_4$ nanoparticles and 5.5 ml 1-butyl-3-methyl-imidazolium hexafluorophosphate ($BMIMPF_6$, IL) were dispersed in 1.8 M HCl solution in a three-neck round-bottomed flask fitted with ultrasonic vibration for 1 h, then 1.8 ml aniline monomer was added to the above mixture, and ultrasonic vibration was continued for another 30 min. The reaction system was then cooled in an ice bath. Under the protection with nitrogen gas, the ammonium peroxydisulfate (4.54 g, dissolved in 1.8 M HCl solution), which serves as an oxidant, was added dropwise into the above mixture with a separatory funnel. The reaction was continued for 12 h at 0 °C under magnetic stirring. The precipitate was centrifuged and washed with water and ethanol 5 times and then dried in a desiccator for further characterization. Other samples were prepared under identical experimental conditions by changing [$CoFe_2O_4$]/[An] molar ratio and oxidant content, the synthesis condition, monomer and oxidant concentrations of different samples can be found in Table 1, the corresponding TG results and analysis can be found in Fig. S1 in supporting information. The PANI–$CoFe_2O_4$ composites with ionic liquid were denoted as PC-A. For comparison, the PANI–$CoFe_2O_4$ composites with no ionic liquid (PC-B) were also prepared by a similar process in the absence of IL.

2.2. Characterization and measurement

The crystal phase of the prepared products were analyzed by X-ray powder diffraction (XRD), employing a scanning rate of 0.02°/s in a 2θ range from 10 to 60° (Model Japan Rigaku D/max-γA K_{α}, Cu-target, $\lambda = 0.1541$ nm). The morphologies and microstructure of the particles and nanocomposite were investigated by transmission electron microscopy (TEM, JEM JEOL-2010). The chemical structure was characterized by a Nicolet 60 SXB spectrophotometer (FT-IR) in which the IR spectra were recorded by diluting the milled powders in KBr. Conductivity was measured by an Agilent 4294A precision impedance analyzer using two polished copper disk electrode sandwich samples. The magnetic hysteresis loop was determined by a vibrating-sample magnetometer (VSM, EG&G Princeton Applied Research Vibrating Sample Magnetometer, Model 155) at room temperature. Thermal gravimetric (TG) analysis was performed with an STA-1200 instrument.

3. Results and discussion

3.1. X-ray diffraction

Fig. 1 shows the XRD patterns of the $CoFe_2O_4$ particles and the PANI–$CoFe_2O_4$ nanocomposites respectively. The $CoFe_2O_4$ powder samples (Fig. 1a) were found to be a spinel structure according to JCPDS Data 22-1086 [26]. Average crystallite size calculated using the Scherer formula is 20.2 ± 1.8 nm. Here λ is the X-ray wavelength, β is the full-width at half maxima (FWHM) of the X-ray diffraction peak, and θ is the Bragg angle. The X-ray diffraction pattern of PC-A is shown in Fig. 1b. A broad peak centered at $2\theta = 22°$ was observed and was ascribed to the scattering from the periodicity parallel and perpendicular to PANI chains [27,28]. The character peaks of $CoFe_2O_4$ are also in this pattern. The relative intensity of $CoFe_2O_4$ was weakened compared with that of the pure composition (Fig. 1a) because of the encapsulation by PANI. Fig. 1c shows the XRD patterns of PC-B, it has almost the same pattern as shown in Fig. 1b. The characterization peaks of $CoFe_2O_4$ and PANI are also found in this pattern.

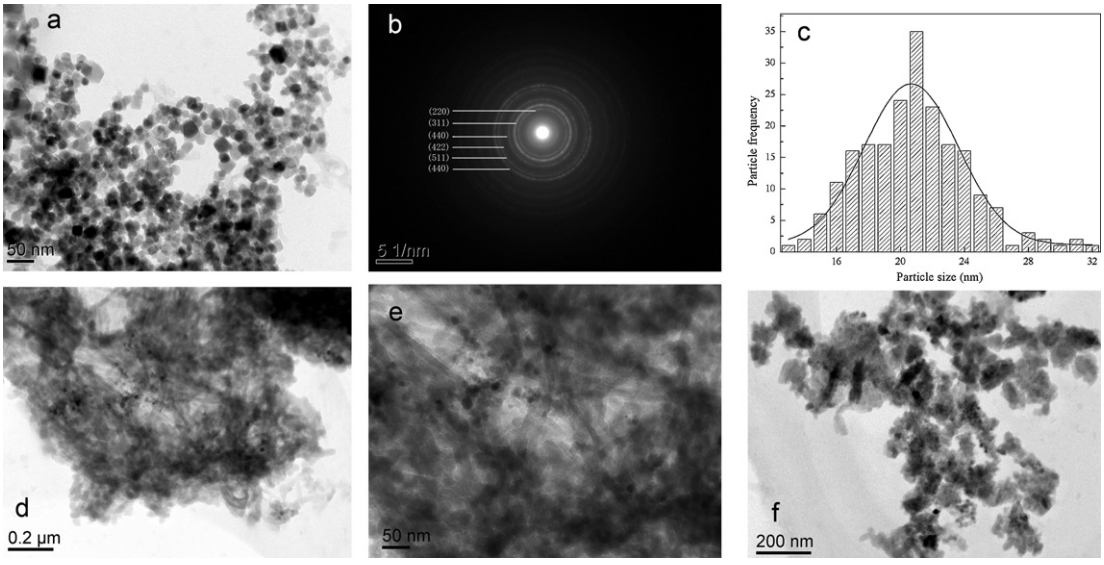

Fig. 2. TEM images of (a) $CoFe_2O_4$ nanoparticles, (b) SAED pattern of (a), (c) The size distribution for the $CoFe_2O_4$ nanoparticles, (d) PC-A, (e) a magnified image of (d), (e) PC-B.

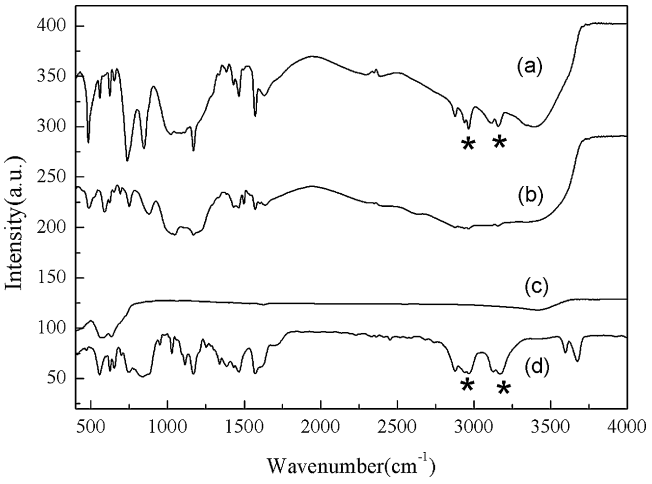

Fig. 3. FT-IR spectra of (a) PC-A, (b) PC-B, (c) $CoFe_2O_4$ particles, (d) $BMIPF_6$.

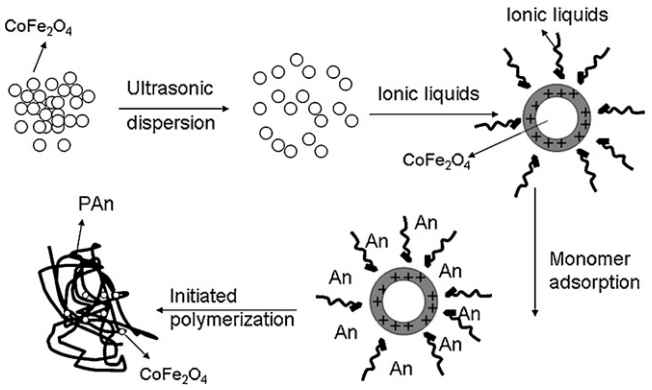

Fig. 4. Formation process of PANI–$CoFe_2O_4$ nanocomposites in ionic liquid.

3.2. Morphology

Fig. 2 shows the TEM images for the $CoFe_2O_4$ nanoparticles and PANI–$CoFe_2O_4$ nanocomposites (PC-A and PC-B), respectively. The $CoFe_2O_4$ particles are spherical in shape with diameters within the range of 15–25 nm. The selected area electron diffraction (SAED) pattern (Fig. 2b) exhibits several diffraction rings which could be indexed to the spinel structure of the $CoFe_2O_4$ particles. The polycrystalline rings are caused by the aggregation of the $CoFe_2O_4$ particles.

Analysis of the TEM image (Fig. 2a) by measuring the diameter of ~200 randomly selected particles in enlarged TEM image, resulting in the particle size distribution histograms (Fig. 2c). The size distribution is found to be well described by a log-normal distribution function from which we obtained the median particle diameter of 20.9 nm for $CoFe_2O_4$ nanoparticles. This result is in good agreement with the XRD analysis.

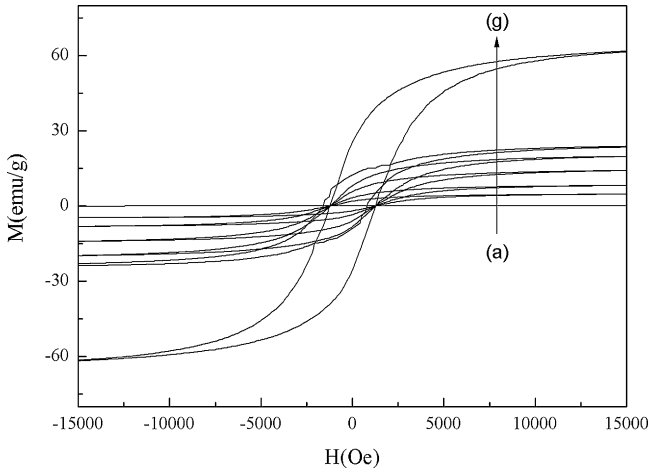

Fig. 5. Dependence of magnetization of PC-A series on $CoFe_2O_4$ concentration with an applied magnetic field at room temperature (a) PANI, weight percentage of $CoFe_2O_4$ is (b) 10 wt%, (c) 20 wt%, (d) 30 wt%, (e) 40 wt%, (f) 50 wt%, (g) $CoFe_2O_4$ nanoparticles.

As shown in Fig. 2(d and e), PANI are nanofibers with about 20 nm in diameter; these nanofibers tend to twist unorderly with each other, indicating that the nanofibers are flexible and are mainly formed at the interface of water and ionic liquid [29,30]. The cobalt ferrite particles were entrapped in the PANI nanofibers during the formation of PANI–$CoFe_2O_4$ composites.

By comparing the morphology of nanocomposites prepared in the absence of ionic liquids (Fig. 2f), two major results were observed: (1) there were no obvious change in the average particle size for $CoFe_2O_4$ with and without $BMIPF_6$, and (2) the degree of dispersion and the uniformity of the resultant composite nanoparticles prepared in the presence of BMIPF6 were effectively improved. For the former, the spherically shaped $CoFe_2O_4$ nanoparticles are discretely dispersed in the PANI nanofibers; for the latter, the PANI are coated or grown on the surface of the magnetic nanoparticles to form core-shell structured electromagnetic functionalized composites. Therefore, $BMIPF_6$, as an anchor agent, played an important role during the synthesis process.

3.3. FT-IR spectra

FT-IR spectra were used to determine the chemical structure of the samples. As shown in Fig. 3. For $CoFe_2O_4$, the peaks at 583 and 574 cm^{-1} can be attributed to Fe–O or Co–O bond [31]. For pure [BMIM] [PF_6] IL, Talaty et al. have also studied [BMIM] [PF_6] and gave the following assignments to the peaks [32]. The peaks at 1571 and 1465 cm^{-1} are attributed to C–N stretching mode; the peak at 1387 cm^{-1} is attributed to C–C stretch mode, and the peak at 857 cm^{-1} is assigned to P–F asymmetric stretch. In the 3000–2800 cm^{-1} range, three peaks at 2966, 2939 and 2877 cm^{-1} can be seen and they arise from the butyl chain can be ascribed to the propyl C–H asymmetric stretch, C–N symmetric stretch and terminal C–H symmetric stretch respectively. For

Table 1
The synthesis condition, monomer and oxidant concentrations of different samples.

[$CoFe_2O_4$]/[An]	Aniline (M)	Oxidant (M)	Temperature (°C)	Synthesis time (h)	Percentage of $CoFe_2O_4$
1:10	0.1	0.1	0	12	10.25%
2:10	0.2	0.2	0	12	19.12%
3:10	0.3	0.3	0	12	31.70%
4:10	0.4	0.4	0	12	39.43%
5:10	0.5	0.5	0	12	47.72%

Note: The percentage of $CoFe_2O_4$ results were generated from the TG measurement analysis.

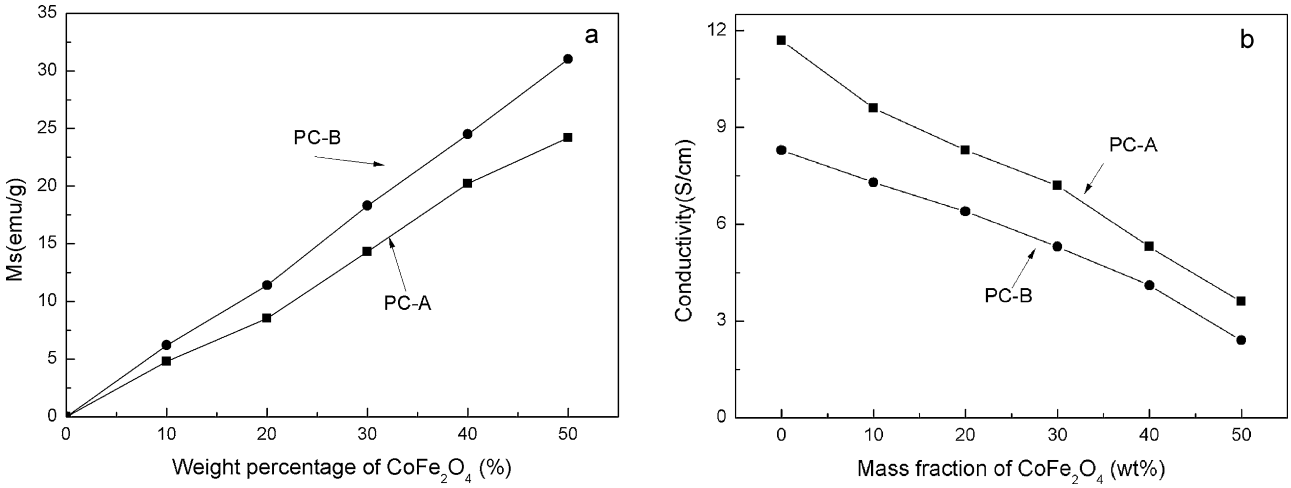

Fig. 6. (a) Magnetization and (b) conductivity of the products prepared at different ratios of $CoFe_2O_4$ and aniline monomer.

vibrations above 3000 cm^{-1} peaks can be seen arising from imidazolium ring emerges at 3170 (ring H–C–C–H asymmetric stretch) and 3126 cm^{-1} (N=C stretch). The observed wavenumbers in our work and in the study of Talaty et al. are not exactly the same but can, nevertheless, be assigned to the same modes [32,33].

For PC-A, the peaks at 1630 and 3410 cm^{-1} can be assigned to the O–H stretching vibrations; the bands at 1568 and 1472 cm^{-1} are attributed to the C=N and C=C stretching modes for the quinonoid and benzenoid units, respectively; the bands at 1290 and 1247 cm^{-1} are attributed to C–N stretching mode for the benzenoid unit; and the band at 1110 cm^{-1} is assigned to an in-plane bending vibration of C–H (mode of N=Q=N, Q=N+H–B and B–N+H–B), which was formed during protonation [34,35]. In addition, the peaks at 583 and 574 cm^{-1} belong to Fe–O or Co–O bond can also be found in the PC-A spectrum. The adsorption of IL onto PC-A was evident from the appearance of the characteristic absorption peak of IL at the spectrum of the PC-A.

By Comparing the FT-IR spectra of PC-A and PC-B, it is interesting to notice that the two are similar with only a few differences. The use of ionic liquid leads to the shift of some bands in the PANI–$CoFe_2O_4$ nanocomposites. For example, the C–N stretching vibrations at 1465 cm^{-1} was shifted to 1452 cm^{-1}, and the in-plane C–H deformation vibration band at 1176 cm^{-1} was shifted to 1168 cm^{-1}. In addition, the characterization peaks from IL around 3175, 3127, 2970, and 2881 cm^{-1} shifted to lower wavenumbers of 3161, 3112, 2963 and 2872 cm^{-1} after IL was introduced. These differences indicate strong interaction between PANI, $CoFe_2O_4$, and ionic liquid in the composites. The interaction between PANI and $CoFe_2O_4$ is thought to be an N-O hydroxyl bond interaction; this makes PANI and $CoFe_2O_4$ difficult to separate. In addition, it can be seen that the peaks in PC-B appear broader than in PC-A, and the intensities are also weakened. These differences are explained according to the constrained growth model of PANI grown in the presence of ionic liquid and $CoFe_2O_4$. In such a case, $BMIPF_6$ acts as an anchor agent surrounding the $CoFe_2O_4$ particles and preventing their aggregation; it acts further as a template, which results in the formation of PANI–$CoFe_2O_4$ nanofiber composites.

The formation mechanism of PANI–$CoFe_2O_4$ nanocomposites (PC-A) is shown in Fig. 4. First, under the ultrasonic vibration, $CoFe_2O_4$ particles will disperse equally into the aqueous solution containing $BMIPF_6$ and to distribute in nanosized particles. $BMIPF_6$ acts as an anchor agent surrounding the $CoFe_2O_4$ particles and prevents aggregation. When $(NH_4)_2S_2O_8$ is added to the mixture, polymerization of the aniline is initiated at the interface of water and $BMIPF_6$; it mainly occurs on the $CoFe_2O_4$ nanoparticle surface, which can be strengthened by hydrogen bonding between the hydroxyl groups on the surface of $CoFe_2O_4$ and –N= in the PANI molecular chains. Finally, PANI was coated to the surface of $CoFe_2O_4$, forming PANI–$CoFe_2O_4$ nanofiber composites.

Fig. 5 shows the dependence of magnetization on $CoFe_2O_4$ nanoparticles content in PC-A nanostructures. (The magnetization curve separately presented can be found in supporting information, Fig. S2). In $CoFe_2O_4$ nanoparticles, saturated magnetization (Ms), remnant magnetization (Mr), and coercive force (Hc) are estimated to be Ms = 63.5 emu/g, Mr = 17.2 emu/g, and Hc = 803 Oe, respectively. The PANI nanoparticles show typical paramagnetic properties due to a spinning polaron, its magnetic moment induced by the applied field is linear in the field strength and rather weak, and its total magnetization drop to zero when the applied field is removed. For PC-A, saturated magnetization increases with increasing the $CoFe_2O_4$ nanoparticles weight percentage, the saturated magnetization is 24.2 emu/g when the mass fraction of $CoFe_2O_4$ is 50 wt%.

Fig. 6a shows the dependence of saturated magnetization on the content of $CoFe_2O_4$ in PANI–$CoFe_2O_4$ nanostructures (PC-A and PC-B series). The saturated magnetization of both series gradually increases with the increased relative content of $CoFe_2O_4$. Contrary to the change in conductivity, the increasing ratio of series A is far less than that of the series B. The saturated magnetization is 24.2 emu/g for the former, but 31.0 emu/g for the latter when the mass fraction of $CoFe_2O_4$ is 50 wt%. The relatively low magnetization may be attributed to the occurrence of a protective layer on the surface of $CoFe_2O_4$ nanoparticles for PC-A. It has been proposed that the positively charged $CoFe_2O_4$ nanoparticles, dispersed in an ionic liquid such as $BMIBF_4$ or $BMIPF_6$, are surrounded by a protective layer [36], which slightly impairs magnetic properties of composites.

Fig. 6b shows the dependence of conductivity on $CoFe_2O_4$ content in PANI–$CoFe_2O_4$ nanostructures (PC-A and PC-B series). The conductivity of both series gradually increases with the decrease of $CoFe_2O_4$ in the nanocomposite. However, the increasing ratio of PC-A series is much faster than that of series B. The conductivity is 9.6 S/cm for the former, but 7.3 S/cm for the latter when the mass fraction of $CoFe_2O_4$ is 10 wt%. The conductivity decreases with the increase of the magnetic nanoparticles content; this can be attributed to partial blockage of the conductivity path by the insulating magnet. The PC-A series has higher conductivity than the B series; it's perhaps that the existence of ionic liquids reduced the intercontact resistance caused by PANI conducting nanofibers enwinding around the $CoFe_2O_4$ magnet. On the other hand, $BMIPF_6$

has ionic conductivity and the synergistic effect of PANI and $BMIPF_6$ results in the improvement of conductivity for the PC-A series.

4. Conclusions

In conclusion, PANI–$CoFe_2O_4$ nanofiber composites were achieved by in situ doping polymerization at the interface of water and ionic liquid. The imidazolium-based ionic liquids $BMIPF_6$ acting as an anchor agent played an important role during the synthesis. For PC-A, the spherically shaped $CoFe_2O_4$ nanoparticles are discretely dispersed in the PANI nanofibers, whereas for PC-B, PANI was coated or grown on the surface of the magnetic nanoparticles to form a core-shell structure. The conductivity of both series gradually decreases with increasing $CoFe_2O_4$ in the nanocomposites; however, the decrease ratio of PC-A is faster than that of PC-B. The saturated magnetization of both series gradually increases with the increased relative content of $CoFe_2O_4$ in the nanocomposites. Contrary to the change in conductivity, the increase ratio of PC-A is less than that of PC-B.

Acknowledgments

We are grateful for the financial support from the National Program on key Basic Research Project (973 Grant No. 2009CB939704 and 2009CB939705) and the National Natural Science Foundation of China (No. 10974148).

Appendix A. Supplementary data

Supplementary data associated with this article can be found, in the online version, at doi:10.1016/j.jallcom.2010.11.197.

References

[1] C. Lucignano, F. Quadrini, L. Santo, J. Compos. Mater. 42 (2008) 2841–2852.
[2] D. Schlemmer, R.S. Angélica, M.J.A. Sales, Compos. Struct. 92 (2010) 2066–2070.
[3] S. Ameen, M.S. Akhtar, G.S. Kim, Y.S. Kim, O.B. Yang, H.S. Shin, J. Alloys Compd. 487 (2009) 382–386.
[4] B.K. Sharma, N. Khare, S.K. Dhawan, H.C. Gupta, J. Alloys Compd. 477 (2009) 370–373.
[5] M. Amerithesh, S. Aravind, S. Jayalekshmi, R.S. Jayasree, J. Alloys Compd. 458 (2008) 532–535.
[6] L. Wei, Q. Chen, Y.J. Gu, J. Alloys Compd. 501 (2010) 313–316.
[7] F. Hussain, M. Hojjati, M. Okamoto, R.E. Gorga, J. Compos. Mater. 40 (2006) 1511–1575.
[8] N.Z. Bao, L.M. Shen, W. An, P. Padhan, C.H. Turner, A. Gupta, Chem. Mater. 21 (2009) 3458–3468.
[9] M. Sangmanee, S. Maensiri, Appl. Phys. A 97 (2009) 167–177.
[10] M.V. Limaye, S.B. Singh, S.K. Date, D. Kothari, V.R. Reddy, A. Gupta, V. Sathe, et al., J. Phys. Chem. B 113 (2009) 9070–9076.
[11] R.J. Choudhary, S.K. Kulkarni, J. Phys. Chem. B 113 (2009) 9070–9076.
[12] Y. Cedeno-Mattei, O. Perales-Perezb, Microelectron. J 40 (2009) 673–676.
[13] V. Sunny, P. Kurian, P. Mohanan, P.A. Joy, M.R. Anantharaman, J. Alloys Compd. 489 (2010) 297–303.
[14] J. Alam, U. Riaz, S.M. Ashraf, S. Ahmad, J. Coat. Technol. Res. 5 (2008) 123–128.
[15] O. Yavuz, M.K. Ram, M. Aldissi, P. Poddar, S. Hariharan, J. Mater. Chem. 15 (2005) 810–817.
[16] K. Singh, A. Ohlana, A.K. Bakhshi, S.K. Dhawan, Mater. Chem. Phys. 119 (2010) 201–207.
[17] A.A. Farghali, M. Moussa, M.H. Khedr, J. Alloys Compd. 499 (2010) 98–103.
[18] P. Thomas, K.H. Dwarakanat, K.B.R. Varma, Synth. Met. 159 (2009) 2128–2134.
[19] B. Birsöz, A. Baykal, H. Sözeri, M.S. Toprak, J. Alloys Compd. 493 (2010) 481–485.
[20] B.T. Su, X.W. Zuo, C.L. Hu, Z.Q. Lei, Acta Phys.-Chim. Sin. 24 (2008) 1932–1936.
[21] H.J. Ding, X.M. Liu, M.X. Wan, S.Y. Fu, J. Phys. Chem. B 112 (2008) 9289–9294.
[22] R.D. Rogers, K.R. Seddon, Science 302 (2003) 792–793.
[23] Z. Ma, J.H. Yu, S. Dai, Adv. Mater. 22 (2010) 261–285.
[24] A. Kumar, S. Murugesan, V. Pushparaj, J. Xie, C. Soldano, G. John, O. Nalamasu, P.M. Ajayan, R.J. Linhardt, Small 3 (2007) 429–433.
[25] J.M. Pringle, O. Ngamna, C. Lynam, G.G. Wallace, M. Forsyth, D.R. MacFarlane, Macromolecules 40 (2007) 2702–2711.
[26] JCPDS Powder Diffraction File, International Center for Diffraction data, Newtown Square, PA, 1980.
[27] J.M. Pringle, O. Ngamna, J. Chen, G.G. Wallace, M. Forsyth, D.R. MacFarlane, Synth. Met. 156 (2006) 979–983.
[28] J.X. Huang, S. Virji, B.H. Weiller, R.B. Kaner, J. Am. Chem. Soc. 125 (2003) 314–315.
[29] G. Socrates, Infrared and Raman Characteristic Group Frequencies: Tables and Charts, third ed., John Wiley and Sons Ltd, 2001.
[30] T. Fukushima, A. Kosaka, Y. Ishimura, T. Yamamoto, T. Takigawa, N. Ishii, T. Aida, Science 300 (2003) 2072–2074.
[31] Z.P. Zhou, Y. Zhang, Z.Y. Wang, W. Wei, W.F. Tang, J. Shi, R. Xiong, Appl. Surf. Sci. 254 (2008) 6972–6975.
[32] E.R. Talaty, S. Raja, V.J. Storhaug, A. Dölle, W.R. Carper, J. Phys. Chem. B 108 (2004) 13177–13184.
[33] M. Wagner, C. Kvarnström, A. Ivaska, Electrochim. Acta 55 (2010) 2527–2535.
[34] G. Socrates, Infrared and Raman Characteristic Group Frequencies, Tables and Charts, third ed., John Wiley & Sons Ltd, 2001.
[35] Z.M. Zhang, M.X. Wan, Y. Wei, Nanotechnology 16 (2005) 2827–2832.
[36] C.C.O. Flavia, L.M. Rossi, R.F. Jardim,.J.C. Rubim, J. Phys. Chem. C 113 (2009) 8566–8572.